The adsorption sites of rare gases on metallic surfaces: a review

2004 J. Phys.: Condens. Matter 16 S2839

(http://iopscience.iop.org/0953-8984/16/29/001)

INSTITUTE OF PHYSICS PUBLISHING JOURNAL OF PHYSICS: CONDENSED MATTER

J. Phys.: Condens. Matter **16** (2004) S2839–S2862 PII: S0953-8984(04)80466-1

The adsorption sites of rare gases on metallic surfaces: a review

R D Diehl[1], Th Seyller[1], M Caragiu[1], G S Leatherman[1], N Ferralis[1], K Pussi[2], P Kaukasoina[2] and M Lindroos[2]

[1] Physics Department, Penn State University, University Park, PA 16802, USA
[2] Institute of Physics, Tampere University of Technology, PO Box 692, Tampere, Finland

Received 4 May 2004
Published 9 July 2004
Online at stacks.iop.org/JPhysCM/16/S2839
doi:10.1088/0953-8984/16/29/001

Abstract

During the past six years, the adsorption geometries of several rare gases in structures having several different symmetries on a variety of substrates were determined using low-energy electron diffraction (LEED). In most of these studies, a preference is found for the rare gas atoms to adsorb in the low-coordination sites. Only in the case of adsorption on graphite has a clear preference for a high-coordination site for a rare gas atom been found. This unexpected behaviour is not yet completely understood, although recent density functional theory (DFT) calculations for these and similar surfaces suggest that this is a general phenomenon. This paper reviews the early studies that were presages of the discovery of top site adsorption for rare gases, the discovery itself, and the present state of understanding of this curiosity. It also details some of the features of the LEED experiments and analysis that are specific to the case of rare gas adsorption.

1. Introduction

The field of physisorption began in the early part of the 20th century with the pioneering work of Langmuir [1]. Physisorbed gases were often used to measure the surface areas of porous materials by measuring the amount of gas adsorbed, with the assumption that the area per adsorbed molecule was independent of the substrate [2]. Later studies showed that the density of the adsorbed molecules or atoms was often affected by the substrate structure. As techniques were developed to study the structures of adsorbates, it was found frequently that adsorbed gases adopted commensurate structures, where each adsorbed atom or molecule occupied an identical adsorption site. Because these weak adsorption bonds were believed to be dominated by the non-directional dispersion forces between the adsorbing atoms and substrate, sites that maximize the coordination of the adsorbate atom or molecule were expected. Until 1990, there appeared to be no cracks in this picture of physisorption.

In the 1970s, experimental methods were developed to study the structures of physisorbed layers, and in the 1980s, techniques involving the scattering of thermal energy He atoms from surfaces played an important role in promoting the understanding of physisorption. Not only did they provide new information on the He–surface interaction through the measurement of scattered intensities, they also provided a method for studying the low-energy vibrations of weakly bonded (physisorbed) species on surfaces. Together these techniques allowed unprecedented precision in the determination of physisorption potentials [3, 4], although they did not, in general, produce information on the adsorption geometry. The development of theoretical models and methods for the describing interactions in physisorption systems paralleled the experimental progress, and the background and culmination of this experimental and theoretical body of work are recounted in a monograph published in 1997 [5]. The measurement of adsorption geometries is a more recent development, and these studies have been carried out mainly using low-energy electron diffraction (LEED). This review will describe the earliest observations related to low-coordination adsorption, the (sometimes) convoluted path of progress, and the current state of understanding of this phenomenon.

2. Historical perspective

Prior to 1990, it was generally assumed that the adsorption potential for rare gas atoms on surfaces would be more attractive in high-coordination sites and less attractive in low-coordination sites. (Figure 1(a) shows a diagram of several types of surface structures and identifies the various sites on a close-packed surface.) Indeed, much of the interest in physisorbed gases arose from the effect on the adsorbed film of the delicate balance of interactions created by the relatively weak interadsorbate interaction and the lateral variation of the adsorption potential energy. The many available combinations of symmetries and relative strengths of interactions meant that physisorbed films could provide numerous realizations of 2D and quasi-2D phenomena, including commensurate and incommensurate phases and the transitions between them, order–disorder and melting transitions, the structures and dynamics of domain wall systems, and simply the effects of a periodic potential on a 2D elastic medium [6]. While the theoretical modelling of such phenomena did not depend on the spatial correspondence of the adsorption potential to the positions of the substrate atoms, such assumptions generally were made when interpreting the experimental results, and the overriding expectation was that physisorbed atoms would favour high-coordination sites.

One prediction made before 1990 was a harbinger of the discovery of low-coordination adsorption sites for rare gases. This was the prediction that in certain cases, the potential experienced by He atoms scattered from surfaces is anticorrugated with respect to the atomic positions [7–9]. This counter-intuitive picture of the He–surface interaction was attributed to the hybridization of the He 1s level with the unoccupied antibonding states in the metal, which are mainly at the positions of the metal atoms. The extra attraction afforded by this hybridization was large enough to cause the He atom to experience a stronger attractive force when it was above a surface atom. This effect was verified experimentally in 1993 for He-atom scattering from a Rh(110) surface [10]. It was noted in a later theoretical study that even if the potential is anticorrugated for an atom that scatters from a surface, this is not necessarily the case for an atom that adsorbs on a surface, since the two processes typically experience different parts of the gas–surface potential energy [11]. This effect recently has been verified and examined in more detail in another theoretical study [12].

The first suggestion of a preference for low coordination for an *adsorbed* rare gas came from the analysis [13] of the He-atom diffraction from the uniaxially compressed phase of Xe on Pt(111) [14]. This structure forms at low temperatures ($T < 60$ K) and

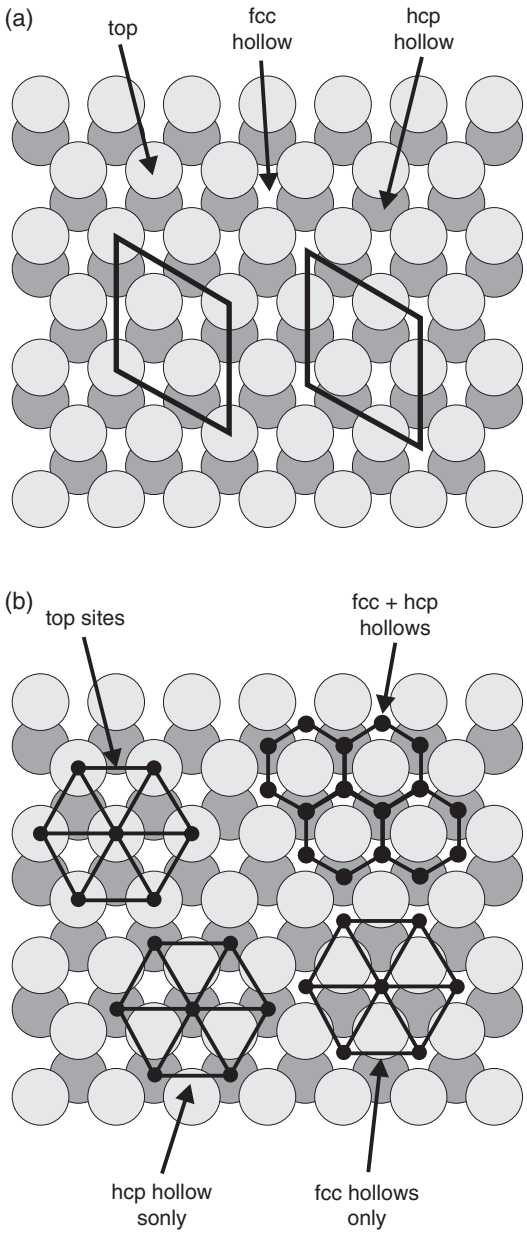

Figure 1. (a) A schematic diagram showing the different types of adsorption sites on an fcc(111) or hcp(0001) surface, and unit cells for the $(\sqrt{3} \times \sqrt{3})R30^\circ$ structure. Only the top two layers of atoms are shown. The unit cells are shown for top site (left) and fcc site (right) adsorption. (b) Adsorption site arrays generated by top sites and hollow sites. If only one type of site is preferred (top, fcc, or hcp), the array is triangular. If both fcc and hcp sites are equally preferred, the array is honeycomb.

consists of a quasihexagonal Xe monolayer on the Pt(111) surface. Because the structure is incommensurate, the Xe atoms in a uniform-density overlayer would have different local geometries with respect to the substrate, and most of these local geometries are not the equilibrium position for a single Xe atom; therefore most Xe atoms experience a lateral force in this structure. The response of the Xe atoms to these forces creates a density modulation in the Xe overlayer that is directly related to the symmetry of the substrate potential. For fcc(111) surfaces, the symmetry of the substrate potential depends on which sites are most attractive to the Xe atoms. Figure 1(b) shows drawings for the arrays of available adsorption sites for

the top sites and the hollow sites being most attractive, respectively. If top sites are preferred, the array is a simple triangular lattice. If the hollow sites are preferred, the array forms a honeycomb structure. The fcc(111) surface has the added complication that half of the hollow sites have atoms directly beneath them in the next layer of atoms (hcp hollows), whereas the other half do not (fcc hollows). If one considers only one set of the hollows (fcc or hcp), then the adsorption sites form a simple triangular lattice, as for the top sites.

The calculations of Gottlieb and Bruch [13, 15] for the uniaxial incommensurate phase of Xe on Pt(111) represented the adsorbate–substrate interaction with a Fourier amplitude having the symmetry of the adsorption sites (either triangular or honeycomb) and the Xe–Xe interactions with a Lennard-Jones pair potential. The calculation started with the uniform uniaxially compressed overlayer and then allowed movement of the Xe atoms until they experienced zero force. The calculated structure factors for the resulting structures were then compared to the measured diffraction intensities, and it was thus found that the triangular lattice substrate potential corresponded well to the experimental diffraction intensities. The conclusion was that the preferred sites form a triangular, and not honeycomb, array, and such an array could be provided by the top sites or by one (fcc or hcp) set of hollow sites. Because the difference in energy between the hcp and fcc sites was expected to be extremely small, the conclusion of this study was that top site preference was likely. Further investigation suggested that even a inequivalence in the fcc and hcp sites could like to a similar result, however [16]. It should be noted that earlier measurements of the phase diagram and heats of adsorption using He-atom scattering [17] and later laser-induced thermal desorption measurements [18] led to estimates of the barrier to lateral motion of the Xe to be in the 30–60 meV range, which was considered to be quite large for physisorption on a metal surface. It was an astonishing idea that on a surface where the corrugation was apparently large, it was also upside down. (Later measurements for the size of the corrugation for a single Xe atom on Pt(111), based on quasielastic He-atom scattering measurements, were considerably smaller, below 10 meV [19].)

An independent theoretical study of Xe on Pt(111) was published the same year. This study was a density functional theory (DFT) calculation for one or two Xe atoms on a cluster of Pt atoms [20]. The result of the calculation was that the top site was preferred by the Xe atom over the hollow site by about 30 meV, and the interpretation of the electron densities suggested that the primary reason for the top site preference was a hybridization of the Xe 5p orbitals with the unoccupied 5d states near the Fermi level in the Pt(111) surface. Shortly after this study, in 1992, an empirical potential energy function for Xe/Pt(111) was constructed, for which the favoured site for Xe was the top site, at a distance 3.35 Å above the Pt(111) surface [21, 22]. However, just one year later in 1993, a similar empirical construction resulted in a potential for which the equilibrium site was the hollow, at 3.1 Å above the surface [23].

Finally, in 1995, a more direct experimental study was carried out to determine the adsorption geometry of Xe/Pt(111) in the $(\sqrt{3} \times \sqrt{3})R30°$ structure [24]. This experiment utilized spin-polarized low-energy electron diffraction (SPLEED), which is a variation of the conventional LEED technique. The result of this experiment was that Xe occupies the hollow sites on the surface, with equal occupations of the fcc and hcp sites. The same group also carried out a similar experiment for the same structure of Xe/Pd(111), which produced a similar result, i.e. that Xe occupies the hollow sites [25]. At this point, the tide seemed to be turning in favour of hollow site adsorption for Xe on close-packed metal surfaces. However, there were some doubts about these SPLEED results, because the Xe–Pt distance was found to be 4.2 Å, which is much larger than the hard sphere distance of 3.2 Å expected for this geometry. It is also out of line with an earlier LEED study for incommensurate Xe on Ag(111) which found an average Xe–Ag(111) perpendicular distance of 3.55 ± 0.1 Å [26]. The Xe–Pd

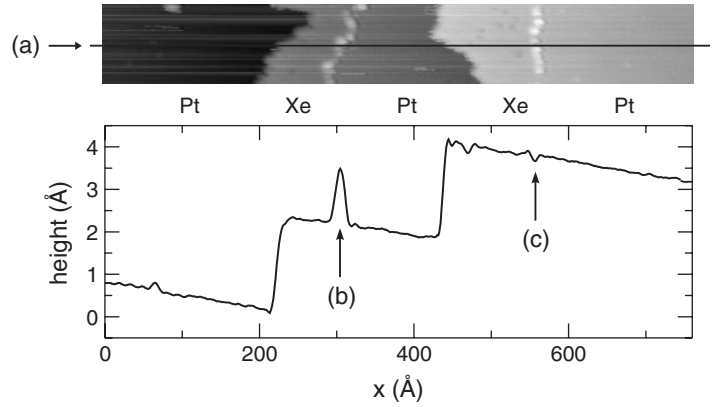

Figure 2. An STM image of Xe adsorbed on Pt(111). The top panel shows the STM image, while the bottom panel shows a line profile across the line labelled (a) in the top panel. The step edges are at the locations of the bright chains in the top panel, and labelled as (b) and (c) in the bottom panel. The bright chains correspond to Xe atoms located at the tops of the step edges. Line (a) passes through a Xe atom at one step edge (b) and between Xe atoms at the other (c). The Xe atoms are not close packed along the step edges.

distance of 3.5 Å for the $(\sqrt{3} \times \sqrt{3})$R30° structure was much more reasonable, based on hard sphere estimates. However, that same study also determined the adsorption geometry for a 'disordered' lower-coverage structure, where Xe was found to be in the top site at a distance of 4.0 Å above the surface. This result also seemed odd since while the low-coverage Xe was thought more tightly bound to the surface, it resided 0.5 Å further away than the Xe in the ordered $(\sqrt{3} \times \sqrt{3})$R30° structure. The difference in the sites at the two coverages was attributed to the tighter bonding in the low-density structure, believed to be a result of the type of hybridization observed in the earlier DFT calculation [20]. It was conjectured that the mutual depolarization resulting from the higher density of atoms at the higher coverage would decrease the hybridization, thus removing the proposed mechanism that supports adsorption in the top sites.

One other tantalizing result reported in 1994 came from a low-temperature scanning tunnelling microscopy (STM) study of Xe on Pt(111) [27, 28]. On this surface, Xe atoms were found to first occupy sites at the locations of defect steps. While the expectation was that Xe atoms would adsorb first at the high-coordination side of the step, just the opposite was found. The first Xe atoms to adsorb were found to reside on top of the step edges, as shown in figure 2. While this result was intriguing and unexpected, it was consistent with the interaction expected between the polarized Xe atoms and the dipole created by the charge-smoothing at the step edge [29]. Both dipoles have their negative end down (toward the bulk) and therefore in the absence of any other interactions, the most attractive location for the Xe atom is the top of the step edge. The repulsive interaction between Xe atoms on top of the step edge was supported by recent temperature programmed desorption data [30]. This interesting observation at step edges does little to elucidate the flat surface situation, however. In the STM images from this study, the islands of Xe that grow from the lower step edges on Pt(111) appear to be normal, dense Xe layers.

Finally, in the mid-1990s two independent groups, in Munich and at Penn State, independently initiated dynamical LEED studies of adsorbed Xe. The Munich group first studied the $(\sqrt{3} \times \sqrt{3})$R30° structure of Xe on Ru(0001) [31], while the Penn State group first studied the same structure of Xe on Cu(111) [32]. The two groups used similar experimental

Figure 3. The LEED pattern at 110 K for Pt(111)–($\sqrt{3} \times \sqrt{3}$)R30°–Xe obtained using a primary beam energy of 290 eV. The pattern was acquired at normal incidence, and the specular beam is obscured by the electron gun in the centre of the screen. The innermost ring of spots corresponds to the first-order scattering from the ($\sqrt{3} \times \sqrt{3}$)R30° superlattice, and the brighter spots in the next ring correspond to the first-order (1 × 1) spots. The threefold symmetry, more apparent at this energy in the higher-order beams, arises from unequal scattering from successive layers of the substrate.

and analysis techniques, and both arrived at the conclusion that the Xe atoms reside on top of the substrate atoms instead of in higher-coordination sites. The Penn State group then went on to study the same structure of Xe on Pt(111) [33] and Pd(111) [34], showing that the conclusions of the earlier SPLEED results were incorrect, and that Xe resides on the top sites on those surfaces [28, 35].

3. Dynamical LEED studies of adsorbed rare gases

3.1. Xe on close-packed surfaces

The details of the Xe adsorption experiments can be found in the individual papers on these studies. A general description of the experiments and their analysis will be given here. Experiments of this type require ultrahigh vacuum, and a sample holder/manipulator that is capable of heating and cooling the sample. For Xe adsorption, the temperature needs to be below about 100 K for adsorption studies, but for LEED studies of these overlayers in general, lower temperatures are better in terms of minimizing the thermal effects in the scattering. Because Xe is weakly bound to the surface (adsorption energy ∼250 meV), the electron beam itself can perturb the layer, although beam effects are not as great for adsorbed Xe as for the lighter rare gases. While an incident beam current of 1 μA might be sufficiently low for an experiment on adsorbed Xe, it is too high for Ar.

A LEED pattern from Pt(111)–($\sqrt{3} \times \sqrt{3}$)R30°–Xe is shown in figure 3. A dynamical LEED experiment involves measuring the integrated intensities of each of the diffraction spots as a function of incident beam energy. Dynamical LEED experiments are most commonly carried out at normal incidence because this allows the averaging of symmetry-equivalent

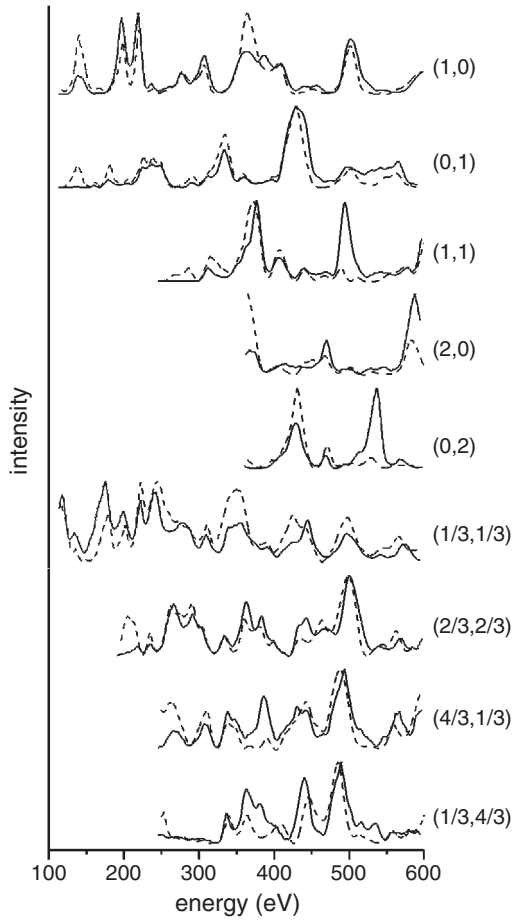

Figure 4. LEED spectra for Pt(111)–($\sqrt{3} \times \sqrt{3}$)R30°–Xe at 80 K. The solid curves are the averaged experimental data and the dashed curves are calculated. The Pendry r-factor for this analysis is 0.33.

beams, thus improving the signal to noise ratio and also reducing the effect of systematic error in the measurement of the incident angle. Figure 4 shows the averaged intensity spectra for the diffracted beams for Xe/Pt(111).

The analysis of such spectra involves the calculation of the scattered electron intensities from model structures for the surface and then the comparison of those spectra to the experimental spectra using a reliability factor or r-factor. The one most commonly used for these types of structure is the Pendry r-factor [36], which emphasizes the locations of the peaks over their relative intensities. For uncomplicated surfaces such as these Xe adsorption structures (i.e. essentially bulk truncation of the substrate and a small, primitive unit cell), the calculation is straightforward using various packaged programs for LEED. The programs we have used are those developed by Van Hove and co-workers [37, 38]. But even though these are rather simple structures, some problematic issues arose during the analyses of these structures. One of these was the ambiguity in the Xe–surface distance, as determined using the Pendry r-factor. This effect, which will be described in some detail below for Xe/Pd(111), was present to some extent for all of the rare gas adsorption structures, although it was most problematic for Xe. The source of the ambiguity is apparently the large perpendicular vibration amplitude of the rare gas atoms, as described later. In spite of the difficulties, however, the level of agreement between the experimental and calculated spectra was generally very good.

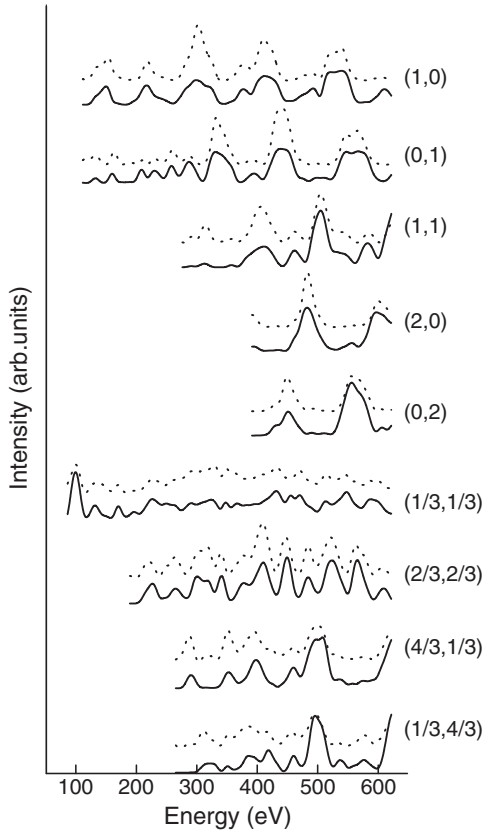

Figure 5. Experimental (solid) and calculated (dashed) spectra for Pd(111)–($\sqrt{3} \times \sqrt{3}$)R30°–Xe. The model used in the calculation has Xe in the top sites and a Xe–Pd perpendicular distance of 3.07 Å. The Pendry r-factor is 0.18.

Here we will briefly describe the analysis for Xe/Pd(111) [34], and then we will summarize and compare the results of the four studies of Xe on close-packed surfaces, which are very similar to each other. The analysis for Xe/Pd(111) was begun by calculating the spectra for different adsorption sites and comparing those to the experimental data. In this analysis, the total length of the data set is 3500 eV, comprising results for nine non-equivalent beams. The adsorption sites that were tested were the top site, fcc hollow, hcp hollow, and a mixture of hcp and fcc sites. In the mixture, the relative fraction of Xe atoms in fcc versus hcp sites was also optimized. Aside from the structural parameters (interlayer spacings, intralayer rumpling), the real and imaginary parts of the inner potential and parameters relating to the vibration amplitudes were optimized. The Pendry r-factor, mentioned above, is 0 for perfect agreement and 1 for uncorrelated spectra. The results of these optimizations are shown in table 1.

The results in table 1 indicate that the top site geometry decisively produces the best fit between the experimental and calculated spectra. Generally, the fractional order beam r-factor gives a greater discrimination between models because the integer order beams, at least in the case of Xe adsorption, are strongly influenced by the substrate structure. Figure 5 shows the LEED spectra for the top site geometry. These spectra correspond to a Xe–Pd spacing of 3.08 Å, and while there is clearly good agreement between the experimental and calculated spectra, it turns out that the agreement is almost as good for other Xe–Pd spacings. This is demonstrated in figure 6. In this figure, Pendry r-factor values are shown which were obtained by changing the Xe–Pd distance while keeping all the other parameters constant. The r-factor clearly shows an oscillatory behaviour with clear minima at Xe–Pd distances of 2.55, 3.05,

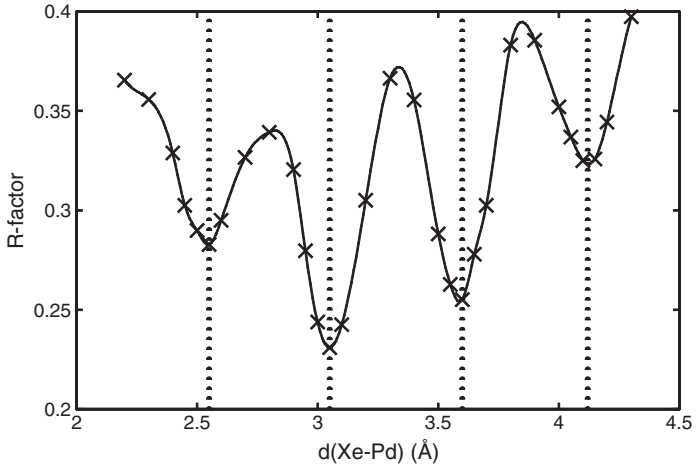

Figure 6. Pendry r-factor as a function of Xe–Pd distance in the model structure for Pd(111)–($\sqrt{3} \times \sqrt{3}$)R30°–Xe. These values are not fully optimized and therefore are somewhat higher than the values given in table 2.

Table 1. Optimum Pendry r-factors for different structure models for Pd(111)–($\sqrt{3} \times \sqrt{3}$)R30°–Xe. Both the overall Pendry r-factor (from all beams) and the fractional order r-factor (from fractional order beams) are given.

Model	R_{Pendry}	$R_{fractional}$
Top	0.18	0.22
fcc hollows	0.47	0.75
hcp hollows	0.47	0.70
60% Fcc +40% Hcp	0.40	0.61

Table 2. Optimized Pendry r-factors for the four minima shown in figure 6.

Xe–Pd spacing (Å)	R_{Pendry}
2.56 ± 0.1	0.22
3.07 ± 0.06	0.18
3.61 ± 0.06	0.18
4.12 ± 0.08	0.23

3.60, and 4.10 Å. Thus, while there is no doubt about the site, there is some ambiguity in the actual geometry. The existence of multiple minima in the r-factor as a function of interlayer spacing is not unique—it arises from the restoration of the constructive interference conditions each time the interlayer spacing is changed by $1/2$ wavelength. In most cases there is one dominant minimum, but in the case of Xe adsorption, there are often several minima having similar values. The case presented here, for Xe/Pd(111), is the most ambiguous case of which we are aware, and presents a good model for use in discussing this effect.

In order to test each of these minima to the fullest extent, the parameters of the individual models were re-optimized, producing the results presented in table 2. Clearly, the difference in the level of fit between the minima provides insufficient discrimination between them. However, the largest and the smallest Xe–Pd distances given here are unphysical, when compared to the Xe–Pd hard sphere distance of 3.56 Å, and they may be ruled out on that

Table 3. r-factors for individual beams for two of the minima given in table 2. The beam indices are given in the top row. The lower r-factor is shown in bold-face type.

d_{Xe-Pd} (Å)	(1, 0)	(0, 1)	(1, 1)	(2, 0)	(0, 2)	(1/3, 1/3)	(2/3, 2/3)	(4/3, 1/3)	(1/3, 4/3)
3.07	**0.128**	0.179	**0.142**	**0.094**	**0.114**	**0.149**	**0.127**	**0.305**	0.338
3.61	0.163	**0.151**	0.160	0.113	0.155	0.154	0.172	0.350	**0.227**

Table 4. Structural parameters determined for the $(\sqrt{3}\times\sqrt{3})$R30° structure of Xe on close-packed surfaces. The parameters are the experimental temperature T, the hard sphere Xe–substrate distance d_{hs}, the measured Xe–substrate distance d_{Xe-sub}, the difference Δ between the hard sphere distance and the measured distance, the degree of first-layer substrate rumple determined in the experiment, δ, the substrate interlayer spacings d_{12}, d_{23}, and d_{34}, the bulk interlayer spacing [57], the Pendry r-factor for this analysis, the heat of adsorption q, and the length of the data set, in eV, of the experimental data. Length dimensions are in Å.

Substrate	T (K)	Site	d_{hs}	d_{Xe-sub}	Δ	∂	d_{12}	d_{23}	d_{34}	d_{bulk}	R_P	q (meV)	Data (eV)
Cu(111)	50	Top	3.47	3.60 ± 0.08	+0.13	0.01 ± 0.02	2.07 ± 0.02	2.06 ± 0.02	2.08 ± 0.03	2.08	0.21	200 [5, 58]	3350
Ru(0001)	20	Top	3.54	3.54 ± 0.06	0.00	0.01 ± 0.04	2.07 ± 0.03			2.14	0.27	230 [59]	2280
Pt(111)	110	Top	3.58	3.4 ± 0.1	−0.18	0.01 ± 0.02	2.29 ± 0.03	2.28 ± 0.04	2.27 ± 0.04	2.26	0.30	260–280 [27, 28]	1900
Pd(111)	77	Top	3.56	3.07 ± 0.06	−0.49	0.02 ± 0.03	2.26 ± 0.03	2.24 ± 0.02	2.24 ± 0.02	2.25	0.18	320 [40]	3500

basis. While using different r-factors [39] often provides another means of discriminating between the results, in this case they did not, because the calculated spectra at these minima are almost identical to each other. Sometimes increasing the data set size can also improve discrimination, but in this case the data set is already quite large (3500 eV), and extending the data to energies higher than 600 eV introduces new problems associated with increasing the size of the calculation. Therefore, in order to discriminate between the remaining two minima in this case, the r-factors of each individual beam were compared for the two structures. These r-factors are given in table 3. It can be seen that for seven of the nine beams, the 3.07 Å structure has the lower r-factor, whereas for two of the beams, the 3.61 Å structure has the lower r-factor. This comparison provides some weight in favour of the 3.07 Å distance. Although it would be considerably more satisfactory if additional discrimination were possible from the experimental data, additional motivation for choosing the 3.07 Å distance comes from comparing the Xe–surface distances obtained from the other studies and the adsorption energies. These data are shown in table 4. It can be seen that the Xe–surface distance is monotonically inversely related to the adsorption energy for adsorption on Cu, Ru, and Pt. An adsorption distance of 3.61 Å for Xe/Pd does not fit into this sequence. Therefore, while it is impossible to definitely rule out the 3.6 Å distance from the diffraction analysis, we have reported 3.07 ± 0.06 Å as the result of this study based on the adsorption energy. The geometrical parameters determined in this study are shown in figure 7. This level of ambiguity in an adsorbate–substrate distance is rather unusual in a LEED experiment, and here we digress to provide a possible explanation for it in the case of Xe adsorption.

The perpendicular vibration amplitude for physisorbed gases is larger than for most adsorbates due to the weak physisorption bond. The scattering electron interacts with the adsorbed atom over a much shorter timescale than the vibration frequency, meaning that any given electron wave will sample adatoms at many heights that can vary by several tenths of

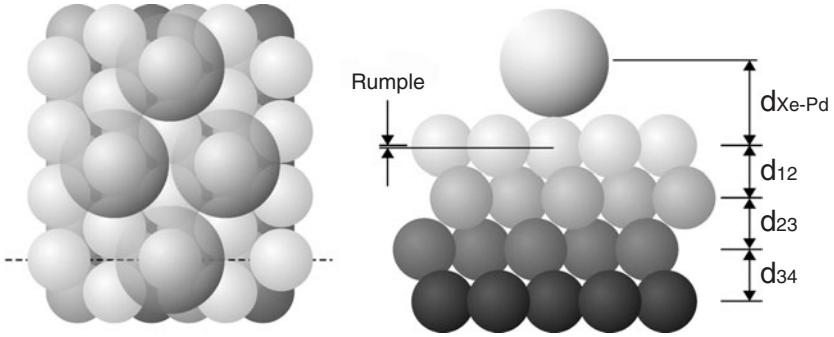

Figure 7. A schematic diagram showing the structural parameters optimized during the LEED analysis for Xe/Pd(111). The dashed line on the left shows the view plane for the drawing on the right.

an Ångstrom. The result of this in terms of the LEED analysis is a broadening of the r-factor minimum as a function of perpendicular distance. The r-factor oscillations shown in figure 6 occur on top of a more general minimum in the r-factor. Ordinarily this general minimum is narrow, and there is just one clear minimum in the function, as shown in figure 8(a). When this general minimum is broadened, as in the case of adsorbed Xe, several minima having similar values can be present, as seen in figure 8(b). This problem of a broad 'best-fit' condition is not restricted to LEED and may occur for other interference-based techniques, but to our knowledge there are no other determinations of Xe–surface geometry using other techniques.

An interesting question is why the SPLEED experiments produced completely different results for the Xe on Pt(111) [24] and Pd(111) [25] systems. In the case of Pt(111), we have noted that the result was for hollow site adsorption at a Xe–surface distance of 4.2 Å, far larger than the distance expected from the hard sphere calculation. While the 4.2 Å distance appears to be the best-fit structure, it was noted that another reasonable fit was found for the top site at a distance of 3.6 Å, but was discarded because it was not the best fit. The method for the determination of the 'best fit' differs in SPLEED and LEED experiments, but perhaps the most significant difference in these studies is in the size of the data set, which typically included only one non-integer beam in the case of the SPLEED measurements. In the case of Pd(111), the adsorption distance of 3.5 Å was not unreasonable compared to the hard sphere distance. This was the deepest minimum for the parameters tested, and no convincing minima were found for any of the top site structures. But Xe–Pd distances smaller than 3.4 Å were apparently not tested for adsorption in the top site. Due to that omission, it cannot be known if the structure found in the LEED study would have produced better agreement in the SPLEED study. We note here that the adsorption geometry found for the 'disordered' phase of Xe on Pd(111) (top site at 4.0 Å) at least found the top site even though the Xe–Pd distance is very large, but this particular phase was not observed in the LEED study described above. A more recent study of this system found that the observed phases and the locations of phase boundaries are very sensitive to impurity concentration [40].

The final geometrical parameters determined for Xe on close-packed substrates are given in table 4. The adsorption site in each case is the top site, and there are no significant changes in the substrate structure compared to the bulk. The Xe–substrate distance depends on the adsorption energy, ranging from 0.13 Å greater than the hard sphere distance (calculated from the nearest neighbour distances in the bulk materials) for Cu to 0.49 smaller for Pd.

The vibration amplitudes deduced from the LEED analysis are given in table 5. In the cases where the vibrations were treated as anisotropic, the vibration amplitudes parallel to

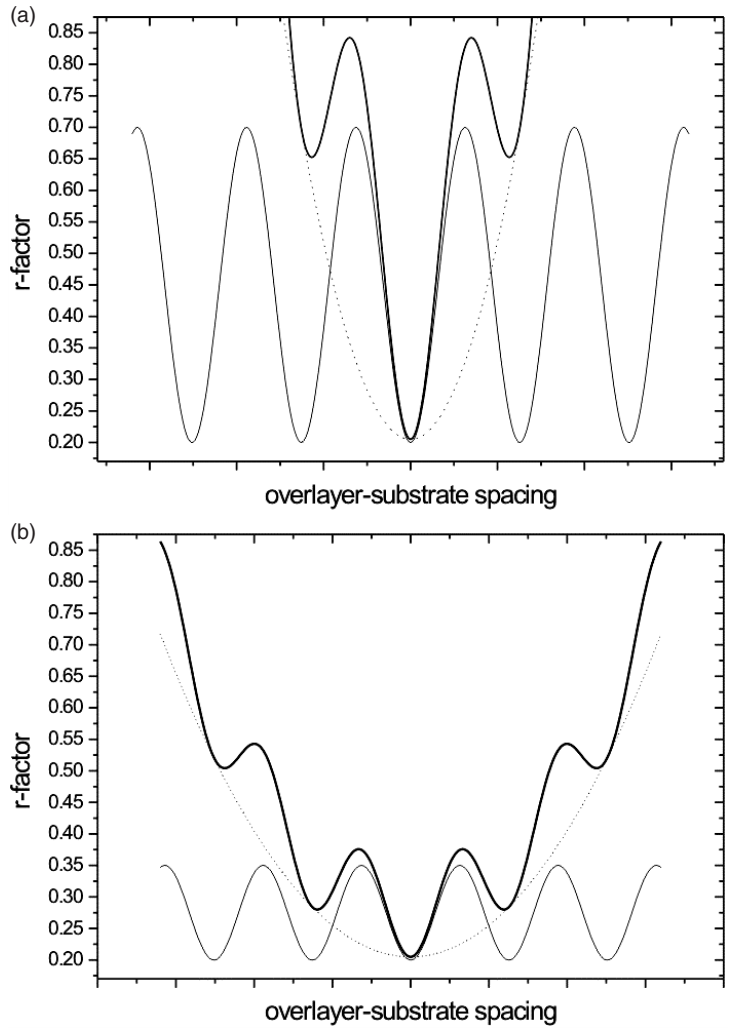

Figure 8. A schematic diagram of the effect of perpendicular thermal disorder on the r-factor as a function of overlayer–substrate distance. (a) Small vibration amplitude: the overall minimum (dashed curve) is narrow; (b) large vibration amplitude: the overall minimum is broad.

the surface were found to be about twice the amplitudes perpendicular to the surface. This is presumably because the lateral Xe interaction is significantly weaker than the Xe–substrate interaction, although the magnitude of the difference in amplitude is rather surprising. By using

$$\frac{1}{2}m\omega_{\perp}^{2}\langle z^{2}\rangle = \frac{\bar{E}}{2} = \frac{k_{\mathrm{B}}T}{2}$$

where $\omega_{\perp}$ is the perpendicular vibration frequency and $\langle z^{2}\rangle$ is the mean square perpendicular vibration amplitude, it is possible to obtain an estimate of the perpendicular vibration energy $E = \hbar\omega_{\perp}$, allowing a comparison to other experiments. The values for the vibration energy obtained in this way are not very precise compared to those obtained using He-atom scattering, but their magnitudes are similar, as seen in table 5. In some LEED analyses, the (likely

Table 5. Measured vibration amplitudes (parallel, perpendicular, isotropic) for adsorbed rare gases. (Note that most of the vibration amplitudes reported in this table are smaller than those reported in the corresponding papers by a factor of $\sqrt{3}$. The vibration amplitude calculated in the dynamical LEED programs must be reduced by a factor of $\sqrt{3}$ to produce 1D amplitudes that can be compared to the 1D oscillator energy equation given in the text. 'Isotropic' corresponds to one component of a vibration amplitude that was modelled as isotropic in the LEED analysis.) Also, deduced vibration energies calculated as described in the text. The final columns give perpendicular vibrational mode energies measured using He-atom scattering, where available. All amplitudes are in Å and the vibration energies are in meV.

System	Temperature (K) (LEED)	Perpendicular	Parallel	Isotropic	Energy (LEED)	Energy (HAS)	Temperature (HAS) (K)
Xe/Cu(111) [32]	50	0.13 ± 0.06	0.29 ± 0.14		$2.8^{+2.5}_{-0.9}$	2.6 [60]	70
Xe/Ag(111) [61]	45	0.11 ± 0.01			$3.2^{+0.3}_{-0.3}$	2.79 [62]	24
Xe/Ru(0001) [48]	20	0.16	0.20		1.5		
Xe/Pt(111) [33]	80	0.17 ± 0.06	0.23 ± 0.06		$2.8^{+1.2}_{-0.7}$	3.40 [63]	80
Xe/Pt(111) [33]	110	0.17 ± 0.06	0.35 ± 0.06		$3.1^{+1.4}_{-0.9}$	3.40 [63]	80
Xe/Pd(111) [34]	77			0.14 ± 0.06	$3.1^{+2.1}_{-0.9}$		
Xe/Cu(110) [64]	20			0.11 ± 0.06	$2.1^{+2.1}_{-1.4}$	2.55 [65]	20
Kr/Cu(110) [66]	25			0.11 ± 0.2[a]	$3.0^{+0.6}_{-0.5}$	2.8 [67]	20
Kr/Ag(111) [61]	30	0.08 ± 0.01			$4.5^{+0.6}_{-0.5}$	2.92 [62]	24
Ar/Ag(111) [45]	31			0.17 ± 0.06	$3.1^{+1.4}_{-0.9}$	3.67 [68]	21
Xe/graphite [49]	57			0.12 ± 0.03	$3.3^{+1.1}_{-0.7}$	3.2 [69], 3.5 [70]	60 20

[a] The value for Kr/Cu(110) has been corrected from the previously published value.

anisotropic) amplitudes are treated as being isotropic [37], but the values thus obtained are dominated by the perpendicular values because the momentum transfer in LEED is mostly in the perpendicular direction. For systems where the amplitude was treated isotropically, the comparison in table 5 uses a 1D component of this amplitude. In retrospect, a better way to determine the thermal properties of a monolayer using LEED may be to deduce a Debye temperature from a temperature dependent measurement of the intensity scattered from the monolayer, and to fix that value in the calculation rather than allowing it to vary as an adjustable parameter, but to our knowledge, this approach has not been used in a dynamical LEED analysis.

4. Xe and Kr on a non-close-packed surface

Since it was not expected that Xe would have a preference for low-coordination sites at all, it was a great surprise that this preference extends to non-close-packed surfaces. The structures of Xe and Kr on Cu(110) had been studied previously using LEED and HAS [41–43]. Both were found to form higher-order commensurate structures that consist of rows of adatoms that are commensurate with the substrate (i.e. one rare gas row per substrate row) and having higher-order commensurate periodicity along the substrate rows. While the structure remains commensurate in the direction across the rows (i.e. remains at one rare gas row per substrate row), the spacing of rare gas atoms along the rows depends on the coverage—as the gas pressure is increased or the temperature decreased, the density along the rows increases. Coincidence (higher-order commensurate) lattices form at certain densities, and these structures provide the opportunity for performing dynamical LEED studies of these structures.

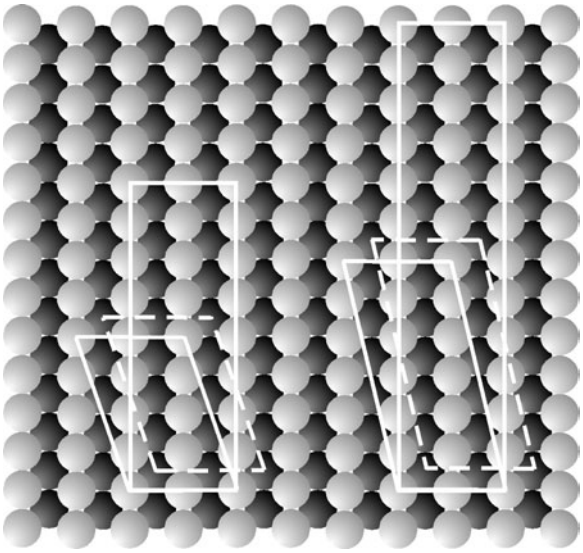

Figure 9. A schematic diagram of the Cu(110) surface and the unit cells for structures observed for Kr (left, c(8 × 2)) and Xe (right, c(12 × 2)) adsorption. The rectangles show the centred unit cell and the rhombuses show the smallest unit cells for these structures. The solid rhombuses show the locations of the corner overlayer atoms if top sites are occupied, and the dashed rhombuses show the locations of the corner atoms if hollow sites are preferred.

Table 6. Structural parameters determined for Xe and Kr on Cu(110). The parameters are the experimental temperature T, the hard sphere bond length d_{hs}, the average overlayer–substrate distance d_{ov-sub}, the substrate interlayer spacings d_{12}, d_{23} and the bulk interlayer spacing [57], the Pendry r-factor, the heat of adsorption q, and the length of the data set, in eV, of the experimental data. Length dimensions are in Å.

Rare gas	T (K)	Site	d_{hs}	d_{ov-sub}	Δ	d_{12}	d_{23}	d_{bulk} (Å)	R_P	q (meV)	Data (eV)
Xe	20	Tops of rows	3.47	3.3 ± 0.1	-0.17	1.19 ± 0.07	1.31 ± 0.07	1.275	0.28	218 ± 6 [71]	4760
Kr	25	Tops of rows	3.28	3.36 ± 0.07	0.08	1.18 ± 0.04	1.31 ± 0.02	1.275	0.18	114 ± 10 [66]	3540

Figure 9 shows the Cu(110) surface with unit cells of two different coincidence structures that form for Kr and Xe adsorption. While the size of the unit cell and the number of atoms per unit cell had been determined in the previous studies, it was not known prior to the dynamical LEED studies whether the rows of Xe or Kr atoms reside in the troughs between Cu rows or on top of the Cu rows. Figure 10 shows the schematic LEED patterns from these higher-order commensurate structures of Kr and Xe. Figure 11 shows the LEED spectra for the case of Kr. For the analysis of these structures, both the tops of rows and the troughs were tested as adsorption locations, and the registry and relaxation of the overlayer atoms along the rows was also tested. In both cases, the best-fit structure had the overlayer atoms on top of the Cu rows. Even though the data sets from these experiments are large (owing to the large unit cell and large number of LEED beams), the number of parameters is too great to get a precise geometry for all of the adsorbed atoms. Although there may be some rumpling and relaxation in the overlayer and/or substrate, the precision is not sufficient for drawing conclusions from these parameters.

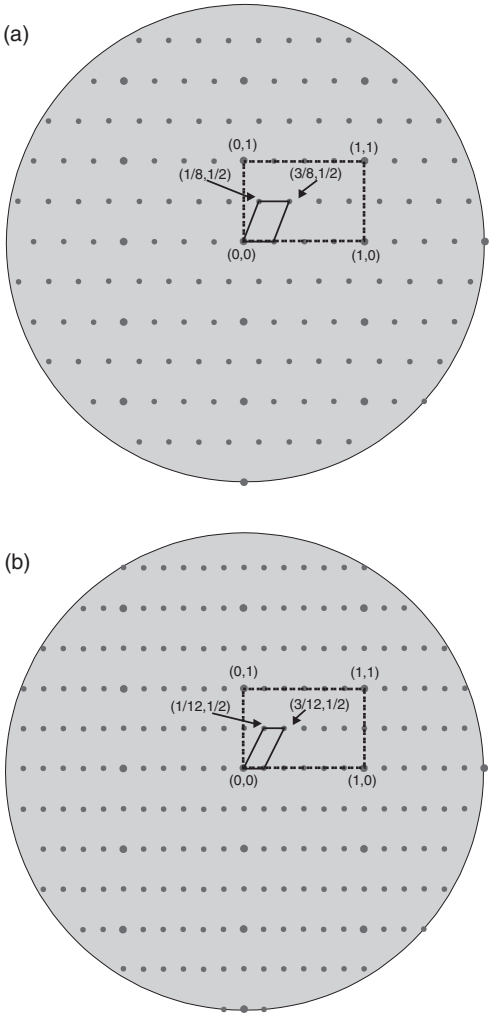

Figure 10. Schematic LEED patterns for (a) Cu(110)–c(8 × 2) and (b) Cu(110)–c(12 × 2). The dashed rectangles denote the substrate unit cells and the rhombuses denote the overlayer unit cells. Representative beam indices are shown.

The most significant result of these studies is that the overlayer atoms are located on the tops of the Cu rows, and the Cu has the same structure as the clean Cu(110) surface. While the dependence of the fit on the registry of the rows of overlayer atoms indicates a preference for a registry where one atom per unit cell is directly above a substrate atom, it is not possible to say whether this implies a preference for top sites, just that there is a clear preference for tops of rows rather than troughs. Figure 12 shows the geometries of the structures determined for Xe and Kr on Cu(110), and table 6 gives the structural parameters.

4.1. Kr and Ar on close-packed surfaces

One of the difficulties with using dynamical LEED to determine adsorption sites is that a commensurate, or at least higher-order commensurate, structure is required, and in the case of

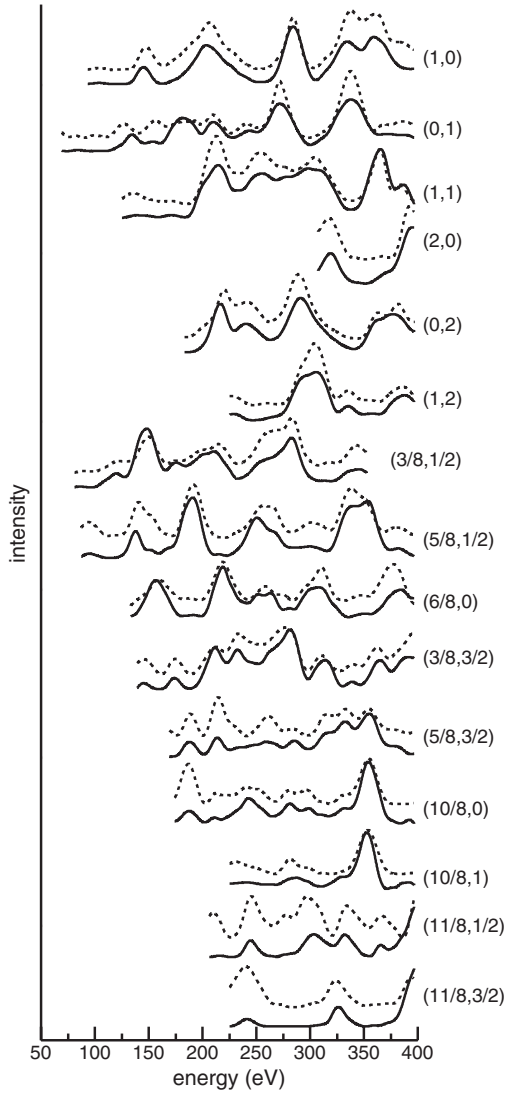

Figure 11. LEED spectra from Cu(110)–c(8 × 2)–5Kr at 25 K. Experimental curves are solid and calculated ones are dashed. The beams are indexed according to the scheme in figure 10(a).

higher-order commensurate structures, knowing the adsorption geometries does not necessarily answer the question of which site is preferred, since more than one site is occupied. On the other hand, because rare gases generally form quasihexagonal-close-packed structures on metal surfaces, it is necessary to find a substrate that matches the rare gas atomic size in order to form a commensurate structure. Finding good matches for simply commensurate structures is not always possible, and therefore higher-order commensurate structures have been used in some cases. Two such structures for adsorption of Kr and Ar on close-packed surfaces are presented here. Both form higher-order commensurate structures with four atoms per unit cell.

Kr adsorbed on Ru(0001) forms a 3×3 structure with four Kr atoms per unit cell. Three model structures consistent with the 3×3 unit cell are shown in figure 13. These structures are those that place adatoms in the highest-symmetry positions, and are drawn so that the corner atoms in the unit cell are in the top, fcc hollow, and hcp hollow sites, respectively. The discrimination between different models was challenging for this structure, but the hcp and fcc

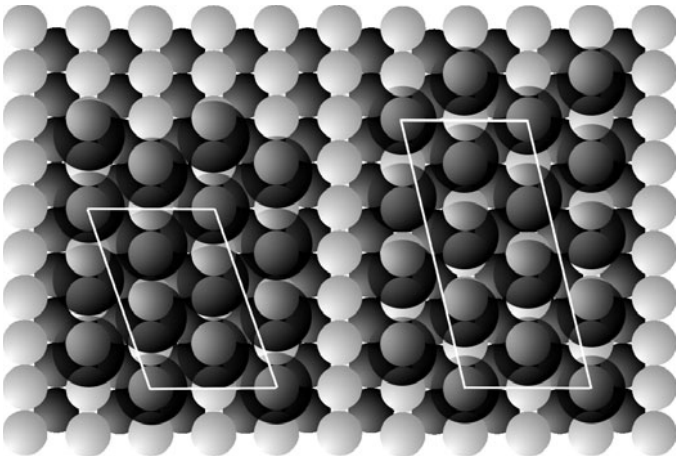

Figure 12. Geometries determined by LEED for Cu(110)–c(8 × 2)–5Kr and Cu(110)–c(12 × 2)–7Xe. See figure 9 for the centred unit cell description.

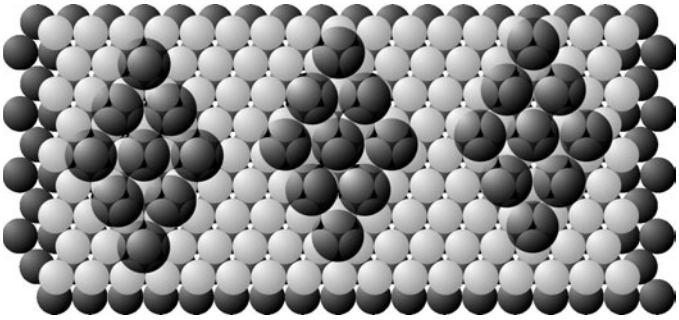

Figure 13. Model surface structures for Ru(0001)–(3 × 3)–4Kr. The left-hand structure has the corner atoms in the top sites, the middle structure has the corner atoms in the hcp hollows, and the right-hand structure has the corner atoms in the fcc hollows.

site models were both found to produce better agreement than the top site structure. Allowing the structure to be populated by domains of both of the hollow site structures improved the fit, and the final best fit was found to comprise 48% fcc and 52% hcp site structures. With the geometry determined, the question is whether this determination provides any information on the preferred adsorption site. However, before discussing this, we will first present the results for Ar/Ag(111).

Ar adsorbed on Ag(111) forms a $(\sqrt{7} \times \sqrt{7})$R19.1° structure with four Ar atoms per unit cell. The structure studied in this LEED experiment is somewhat different from the others presented here because it was found to be necessary to introduce a co-adsorbate into the surface to produce this structure. This is because the hexagonal Ar overlayer lattice always aligns along the substrate lattice symmetry direction on the clean surface, presumably due to pinning at defect step edges [44]. It was found that if a small amount of CO is adsorbed first, then the subsequent Ar layer forms structures that are rotated at other angles. With CO pre-adsorption and for an appropriate Ar density, the Ar overlayer forms a higher-order commensurate $(\sqrt{7} \times \sqrt{7})$R19.1° structure [45].

Two model structures consistent with the $(\sqrt{7} \times \sqrt{7})$R19.1° unit cell are shown in figure 14. What is striking about these structures is that, in terms of local geometries, they are identical to

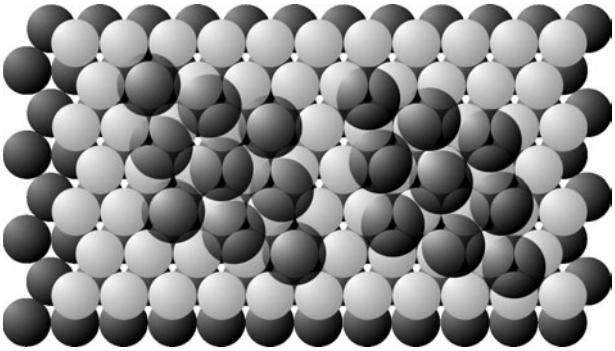

Figure 14. Model structures for Ag(111)–($\sqrt{7} \times \sqrt{7}$)R19.1°–4Ar. The left-hand structure has the corner atoms in the top sites, while the right-hand structure has the corner atoms in the (fcc) hollows.

Table 7. Structural parameters determined for Ru(0001)–(3 × 3)–4Kr and Ag(111)–($\sqrt{7} \times \sqrt{7}$)R19.1°–4Ar. The 'intermediate' site refers to a location between a top and a hollow site (see figure 12). The parameters are the experimental temperature T, the hard sphere adsorbate–substrate bond length d_{hs}, the measured adsorbate–substrate bond length d_{ov-sub}, the difference Δ between d_{hs} and d_{ov-sub}, the measured interlayer spacings of the substrate d_{12} and d_{23}, the bulk interlayer spacing of the substrate [57], the measured rumple in the overlayer ∂, the Pendry r-factor, the heat of adsorption q, and the length of the experimental data set in eV. Length dimensions are in Å.

System	T (K)	Sites/unit cell	d_{hs}	d_{ov-sub}	Δ	d_{ov-sub}	d_{12}	d_{23}	d_{bulk}	∂	R_P	q (meV)	Data (eV)
Kr/	20	1 hollow,	3.38	4.01	0.63	3.70	2.05		2.14	0.02	0.27	152	3055
Ru(0001)		3 intermediate		± 0.03		± 0.03	± 0.03			± 0.03		[59]	
Ar/	31	1 top,	3.30	3.22	−0.08	3.22	2.34	2.37	2.36	0.06	0.32	99	3200
Ag(111)		3 bridge		± 0.07		± 0.07	± 0.04	± 0.07		± 0.08		± 7 [61]	

the (3 × 3) structures shown in figure 13. However, unlike the Kr/Ru(0001) result, the optimum structure found in the LEED analysis for Ar/Ag(111) was the structure with the corner atoms in the top sites. In this structure, one atom per unit cell resides in the top site, while the three others reside in bridge sites. The structural parameters determined in this study and those for Kr/Ru(0001) described above are given in table 7.

Comparing the two structures presented above, several conclusions can be drawn. First, the local structures of the atoms are different in the two cases. In the first case (Kr/Ru) the preferred structure has one atom per unit cell in a hollow site and the other three in positions that are halfway between a top site and a hollow site (see figure 13). In the second case, the preferred structure has one atom per unit cell in a top site, and the other three are in bridge sites (see figure 14). At first glance, this suggests that the two systems are demonstrating a preference for different adsorption sites. Interestingly, the authors in both studies argued that the structure that they found was consistent with a preference for the top site. In the following paragraph, we examine these arguments and present the results of a theoretical study for Ar/Ag(111).

In the Kr/Ru study, the structure was believed to indicate a preference for the top sites, even though no Kr atoms occupy the top sites, and a quarter of them occupy hollow sites. The argument in favour of top site preference was based on the observation that the three atoms per unit cell that were not in hollow sites are near top sites, i.e. they are halfway between top sites and hollow sites. It was also observed that the height of the Kr atoms above the surface is greater for the atoms in the hollow sites than for those in the other sites, by 0.02 ± 0.03 Å

for the fcc sites and 0.03 ± 0.04 Å for the hcp sites. As discussed below, this might be the most important parameter for the determination of adsorption site preference in higher-order commensurate structures such as this. In the case of Ar/Ag, it was argued that the structure indicated a preference for top sites because while one atom per unit cell was in the top site and three were in bridges, there were no atoms in hollow sites. However, in this case, the atoms in the top sites were found to be 0.01 ± 0.06 Å higher (further from the surface) than those in the bridge sites. Aside from being a very uncertain result, there is an added oddity in this determination that the top layer of Ag(111) itself was found to be rumpled, having an amplitude of about 0.06 ± 0.08 Å, with the Ag atoms beneath the top site Ar atoms higher than the others.

Following these experimental studies, a theoretical study for Ar/Ag(111) [46] analysed the origin of the stability of the $(\sqrt{7} \times \sqrt{7})$R19.1° structure. By representing the adatom–substrate potential energy as a truncated Fourier series using the first shell of reciprocal lattice vectors, and by inserting into this potential energy equation experimental values for the heat of adsorption and a force constant deduced from the perpendicular vibration energy, it was determined that the site preference has consequences for the adsorption geometry. Specifically, if the top site is the preferred site, the adatom in the top site will be closer to the substrate than those in the bridge sites, and conversely if the hollow site is preferred, the adatoms in the bridge sites will be closer to the substrate. The expected magnitude of the difference in height is less than 0.1 Å [46]. This qualitative result also had been predicted in a DFT calculation for Ar on Ag(111), where a height difference of 0.15 Å was observed for Ar in top sites compared to bridge sites (with top site Ar atoms closer to the substrate) [47]. Comparing these predictions to the experimental result is not very satisfying since the measured height difference is only 0.01 ± 0.06 Å. However, taking it at face value, it would suggest that the hollow sites are preferred for Ar/Ag(111). Considering the result for Kr/Ru(0001), a similar dependence of the adsorption height on the site preference might be expected, and the result, 0.02 ± 0.03 Å (fcc) or 0.03 ± 0.04 Å (hcp) [48], at face value suggests that the top sites are preferred for Kr/Ru(0001). Obviously it is very desirable to have more precise determinations of this nature in order to further elucidate the effects of site preference on adsorption geometries.

4.2. Xe/graphite

The basal plane of graphite is one of the most widely used substrates for physisorption studies because of its inertness and availability in various forms. The structure of this surface, shown in figure 15, is a honeycomb array of C atoms. In the many thermodynamic studies of rare gases physisorbed on graphite, it was generally assumed that the preferred site is the sixfold-coordinated hollow in the honeycomb structure. This assumption was consistent with pair potential calculations for the adsorption properties. It was not until after the unexpected preference for low coordination was observed for Xe on metal surfaces that the adsorption site for Xe on graphite was investigated experimentally [49]. This LEED study showed that, contrary to the situation on metal surfaces, Xe does indeed occupy the high-coordination sites in the $(\sqrt{3} \times \sqrt{3})$R30° structure, as shown in figure 15.

The optimum structural parameters determined in the LEED study are given in table 8. The adsorption sites tested were the two types of top site (distinguished by whether or not there is a substrate atom directly beneath them in the second layer), the bridge site and the hollow site. The hollow site was clearly favoured, and the Xe–graphite distance was determined to be 3.59 ± 0.04 Å. This corresponds to a Xe–C distance of 3.85 ± 0.04 Å, which is consistent with the sum of the van der Waals radii of C (1.73 Å) and Xe (2.16 Å) [49]. The vibrational

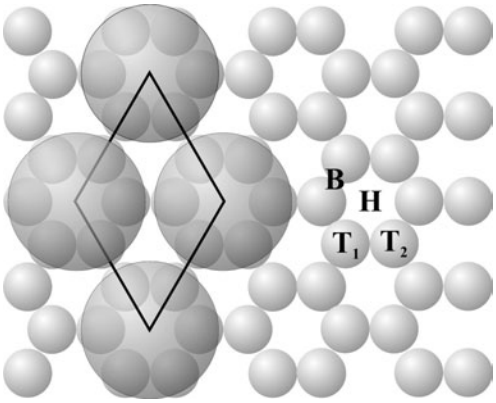

Figure 15. Model structure for graphite(0001)–($\sqrt{3} \times \sqrt{3}$)R30°–Xe. H, B, and T denote hollow, bridge, and top sites, respectively. T_1 and T_2 distinguish the different types of top sites, one of which has a second-layer atom beneath it.

Table 8. Structural parameters determined for graphite(0001)–($\sqrt{3} \times \sqrt{3}$)R30°–Xe. The parameters are the experimental temperature T, the hard sphere adsorbate–substrate bond length d_{hs}, the measured adsorbate–substrate bond length d_{Xe-sub}, the difference Δ between d_{hs} and d_{Xe-sub}, the perpendicular overlayer–substrate spacing d_{ov-sub}, the measured interlayer spacings of the substrate d_{12} and d_{23}, the bulk interlayer spacing of the substrate [57], the Pendry r-factor, the heat of adsorption q, and the length of the experimental data set in eV. Length dimensions are in Å.

T (K)	Site	d_{hs}	d_{Xe-sub}	Δ	d_{ov-sub}	d_{12}	d_{23}	d_{bulk}	R_P	q (meV)	Data (eV)
57	Hollow	3.89	3.85 ± 0.04	-0.04	3.59 ± 0.04	3.33 ± 0.04	3.36 ± 0.09	3.35	0.29	239 [72]	1445

amplitude of the Xe atom was fitted (via the Debye temperature) and optimized to 0.12 Å, as given in table 5.

4.3. Discussion and summary

The results of the experiments presented here indicate that on many metal surfaces, there is a preference for low-coordination adsorption for Xe, Kr, and possibly Ar. This preference is not a weak effect. It extends to non-close-packed surfaces such as Cu(110), and it has been observed on many different metals, indicating that the details of the electronic structure of the metal may not play an important role in the site preference.

Before the first proposals of top site preference in 1990, the assumption of high-coordination preference was based largely on the ideas of pair potentials, non-directional bonding, and the expectation that the atom would penetrate more deeply and experience a more attractive potential in the hollow site. Behind this expectation is the assumption that the repulsive potential at the surface is proportional to the atomic charge density [50, 51]. The natural assumption is that the charge density is highest at the locations of the atoms, but a later DFT study of Ar/Ag(111) [47], questioned this. This study found that the top site was preferred over the hollow site, similar to the DFT result for Xe/Pt(111) [20], but the Ar/Ag(111) study also found the height of the adsorbed atom in the top site to be 0.2 Å smaller than in the hollow site. This was attributed to the delocalization of charge density that increases the repulsive effect at the hollow sites relative to the top site and lifts the potential well upwards both in energy and height. As discussed below, this difference in heights seems to be a key element in the preference for adsorption in the top sites.

In the DFT study of Xe on a Pt(111) cluster, the preference for the top site for Xe/Pt(111) was attributed to a stronger bonding of the Xe to the Pt when in the top site due to a hybridization of the Xe 5p orbitals with the unoccupied d states in the metal, which are localized at the top sites. This interpretation is reminiscent of the arguments made for the anticorrugated He–surface potential discussed earlier [7–9]. Hybridization was also given as the cause for top site preference in another, more recent DFT study of Xe/Pt(111) [52]. More recent DFT calculations for Xe adsorption on many different metal surfaces have produced a somewhat different interpretation, however [53]. In these recent DFT studies, the adsorption of Xe on Cu(111), Pt(111), Pd(111), Mg(0001), Al(111), and Ti(0001) was examined. A greater degree of hybridization for top site adsorption was observed in all cases, and the degree of hybridization was substrate dependent. However, the dominant effect contributing to the site preference was not the hybridization, but the effect of the Pauli repulsion between the Xe atom and the substrate.

Figure 16 shows the calculated potential energy for Xe/Pt(111) in the $(\sqrt{3} \times \sqrt{3})$R30° structure as a function of overlayer–substrate distance [53]. It is clear from this figure that the equilibrium Xe–substrate distance is shorter for the top site. When this potential is decomposed into attractive and repulsive parts, as shown in the figure, it is clear that the biggest difference between the top and hollow sites resides in the repulsive part. Two effects are cited as contributing to this difference, and both effects are linked to the electronic character of the surface that is apparently common to all metal surfaces. This character is the relative donor-like character at the position of surface atoms and the acceptor-like character at the regions between atoms. This characteristic leads to a relative ease for the surface to shift electron charge away from the top site locations. Therefore, when a Xe atom approaches with its dipole pointing negative side down, the extra screening afforded at the top site allows the Xe to increase its dipole moment and its attraction to the surface. This screening also leads to a charge build-up in the hollow site regions that increases the repulsion that allows a closer approach of the Xe atom in the top site. This effect is similar to that proposed earlier for Ar/Ag(111), although in that case, it was presented more as a static effect of delocalization in the metal surface [47]. Recently, another theoretical study has examined the origin of the interface dipole for Xe adsorption and concluded that it was largely due to exchange-like effects rather than hybridization [54].

The recent DFT calculations [53] indicate that the top site is the preferred site for all of the metal surfaces studied. These surfaces are all close packed, and the difference in the adsorption energies for top and hollow sites ranges from about 1 to 50 meV. The smallest difference is for Al(111). Although that structure studied theoretically is unlikely to occur experimentally due to the lattice mismatch, it does suggest that there are metal surfaces, perhaps ones that are not close packed, where Xe prefers the hollow sites. The preference for the top site also has been observed in DFT calculations for Kr and Ar [55] although as the polarizability of the adatom gets smaller, the preference for the top site must decrease, within the picture of this model.

The case of Xe/graphite is the only structure where it is clearly shown that Xe prefers a hollow site. In this case, both the structure and the electronic nature of the surface are quite different from those for the other metals studied. The degree of screening afforded by graphite upon adsorption of Xe is unknown, but is likely to be significantly less because of the semi-metal nature of graphite.

While our understanding of rare gas adsorption has changed radically in the past five years due to the rather sudden influx of experimental studies that show that low-coordination sites are preferred by rare gases on metal surfaces, there are still some issues that are unresolved. The picture of top site preference is still not crystal clear, and it would be useful to have a better understanding of the interaction of rare gases with metal surfaces. The parameters that

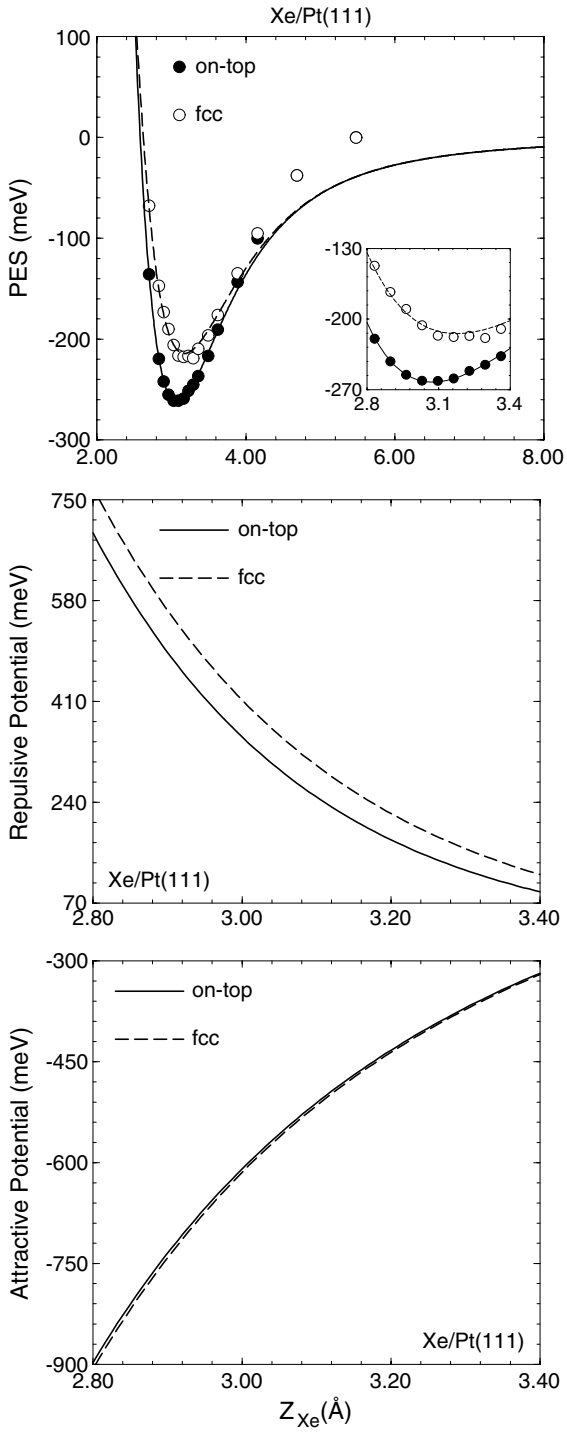

Figure 16. Calculated potential energies for Xe on Pt(111) for top and fcc sites as a function of the distance from the surface [53]. The top panel shows the calculated potential (filled and empty points). The inset shows detail near the minimum. The middle and bottom panels show the decomposition of the fitted curves from the top panel for the repulsive and attractive terms, respectively. The decomposition was performed using the empirical formula $E(z) = A\exp(-Bz) - C(z - z_0)^{-3}$ where z_0 is the position of the image plane [5].

govern adsorption site preference have not been examined, largely because of the apparent difficulty of finding a system that can be studied, experimentally or theoretically, where high-

coordination sites are preferred. The issue of adsorption at step edges was briefly mentioned at the beginning of this review. While Xe has been observed to adsorb on the tops of step edges in some systems [28, 35], it has been observed to adsorb at the bottoms of steps in others [56]. While simulations of these systems have provided new insight [30], there have not yet been any first-principles calculations for such systems. There have been relatively few studies of adsorption geometries for the smaller rare gases, although these are probably better candidates for the observation of high-coordination sites. The reason for the lack of study in this area experimentally is mainly because of the lattice mismatch between the smaller rare gases and most metal surfaces that cause most commensurate structures to have multiple atoms per unit cell, and the characterization and interpretation of such systems is generally complex.

Acknowledgments

We thank L W Bruch, C Stampfl, P Zeppenfeld and J Nieminen for informative discussions, useful critical comments on this manuscript, and, in some cases, supplying figures for this review. We gratefully acknowledge financial support from the National Science Foundation (DMR-0208520 and DGE-9979579).

References

[1] Langmuir I 1918 *J. Am. Chem. Soc.* **40** 1361
[2] Ross S and Olivier J P 1964 *On Physical Adsorption* (New York: Wiley–Interscience)
[3] Hulpke E (ed) 1992 *Helium Atom Scattering From Surface* (Berlin: Springer)
[4] Zeppenfeld P 2001 Noble gases on metals and semiconductors *Landolt–Börnstein: Physics of Covered Surfaces* ed H P Bonzel (Berlin: Springer) p 67
[5] Bruch L W, Cole M W and Zaremba E 1997 *Physical Adsorption: Forces and Phenomena* (Oxford: Oxford University Press)
[6] Shrimpton N D, Cole M W, Steele W A and Chan M H W 1992 Rare gases on graphite *Surface Properties of Layered Structures* ed G Benedek (Amsterdam: Kluwer) p 219
[7] Annett J F and Haydock R 1984 *Phys. Rev.* B **29** 3773
[8] Annett J F and Haydock R 1986 *Phys. Rev.* B **34** 6860
[9] Annett J F 1987 *Phys. Rev.* B **35** 7826
[10] Rieder K H, Parschau G and Burg B 1993 *Phys. Rev. Lett.* **71** 1059
[11] Petersen M, Wilke S, Ruggerone P, Kohler B and Scheffler M 1996 *Phys. Rev. Lett.* **76** 995
[12] Jean H, Trioni M I, Brivio G P and Bortolani V 2004 *Phys. Rev. Lett.* **92** 013201
[13] Gottlieb J M 1990 *Phys. Rev.* B **42** 5377
[14] Kern K, David R, Zeppenfeld P, Palmer R and Comsa G 1987 *Solid State Commun.* **62** 391
[15] Gottlieb J M and Bruch L W 1991 *Phys. Rev.* B **44** 5759
[16] Zeppenfeld P, Comsa G and Barker J A 1992 *Phys. Rev.* B **46** 8806
[17] Kern K, David R, Zeppenfeld P and Comsa G 1988 *Surf. Sci.* **195** 353
[18] Meixner D L and George S M 1993 *Surf. Sci.* **297** 27
[19] Ellis J, Graham A P and Toennies J P 1999 *Phys. Rev. Lett.* **82** 5072
[20] Müller J E 1990 *Phys. Rev. Lett.* **65** 3021
[21] Barker J A and Rettner C T 1992 *J. Chem. Phys.* **97** 5844
[22] Barker J A and Rettner C T 1992 *J. Chem. Phys.* **101** 9202(E)
[23] Rejto P A and Andersen H C 1993 *J. Chem. Phys.* **98** 7636
[24] Potthoff M, Hilgers G, Müller N, Heinzmann U, Haunert L, Braun J and Borstel G 1995 *Surf. Sci.* **322** 193
[25] Hilgers G, Potthoff M, Müller N and Heinzmann U 1995 *Surf. Sci.* **322** 207
[26] Stoner N, Hove M A V, Tong S Y and Webb M B 1978 *Phys. Rev. Lett.* **40** 243
[27] Widdra W, Trischberger P, Friess W, Menzel D, Payne S H and Kreuzer H J 1998 *Phys. Rev.* B **57** 4111
[28] Zeppenfeld P, Horch S and Comsa G 1994 *Phys. Rev. Lett.* **73** 1259
[29] Smoluchowski R 1941 *Phys. Rev.* **60** 661
[30] Lehner B, Hohage M and Zeppenfeld P 2003 *Phys. Rev.* B **65** 165407
[31] Narloch B and Menzel D 1997 *Chem. Phys. Lett.* **270** 163

[32] Seyller T, Caragiu M, Diehl R D, Kaukasoina P and Lindroos M 1998 *Chem. Phys. Lett.* **291** 567
[33] Seyller T, Caragiu M, Diehl R D, Kaukasoina P and Lindroos M 1999 *Phys. Rev.* B **60** 11084
[34] Caragiu M, Seyller T and Diehl R D 2002 *Phys. Rev.* B **66** 195411
[35] Horch S, Zeppenfeld P and Comsa G 1995 *Appl. Phys.* A **60** 147
[36] Pendry J B 1980 *J. Phys. C: Solid State Phys.* **13** 937
[37] Van Hove M A and Tong S Y 1979 *Surface Crystallography by LEED* (*Springer Series in Chemical Physics* vol 2) (Berlin: Springer)
[38] Van Hove M A, Moritz W, Over H, Rous P J, Wander A, Barbieri A, Materer N, Starke U and Somorjai G A 1993 *Surf. Sci. Rep.* **19** 191
[39] Van Hove M A, Weinberg W H and Chan C-M 1986 *Low Energy Electron Diffraction* (*Springer Series in Surface Science* vol 6) (Berlin: Springer)
[40] Zhu J F, Ellmer H, Malissa H, Brandstetter T, Semrad D and Zeppenfeld P 2003 *Phys. Rev.* B **68** 045406
[41] Ramseyer C, Girardet C, Zeppenfeld P, Goerge J, Büchel M and Comsa G 1994 *Surf. Sci.* **313** 251
[42] Glachant A, Jaubert M, Bienfait M and Boato G 1981 *Surf. Sci.* **115** 219
[43] Zeppenfeld P, Büchel M, Goerge J, David R, Comsa G, Ramseyer C and Girardet C 1996 *Surf. Sci.* **366** 1
[44] Leatherman G S, Diehl R D, Karimi M and Vidali G 1997 *Phys. Rev.* B **56** 6970
[45] Caragiu M, Leatherman G S, Seyller T and Diehl R D 2001 *Surf. Sci.* **475** 89
[46] Bruch L W 2001 *Phys. Rev.* B **64** 3407
[47] Kirchner E J J, Kleyn A W and Baerends E J 1994 *J. Chem. Phys.* **101** 9155
[48] Narloch B and Menzel D 1998 *Surf. Sci.* **412/413** 562
[49] Pussi K, Smerdon J, Ferralis N, Lindroos M, McGrath R and Diehl R D 2004 *Surf. Sci.* **548** 157
[50] Esbjerg N and Nørskov J K 1980 *Phys. Rev. Lett.* **45** 807
[51] Nørskov J K and Lang N D 1980 *Phys. Rev.* B **21** 2131
[52] Betancourt A E and Bird D M 2000 *J. Phys.: Condens. Matter* **12** 7077
[53] Da Silva J L F, Stampfl C and Scheffler M 2003 *Phys. Rev. Lett.* **90** 066104
[54] Bagus P S, Staemmler V and Woell C 2002 *Phys. Rev. Lett.* **89** 096104
[55] Stampfl C 2003 private communication
[56] Dienwiebel M, Zeppenfeld P, Einfeld J, Comsa G, Picaud F, Ramseyer C and Girardet C 2000 *Surf. Sci.* **446** L113
[57] Kittel C 1986 *Introduction to Solid State Physics* 6th edn (New York: Wiley)
[58] Vidali G, Ihm G, Kim H-Y and Cole M W 1991 *Surf. Sci. Rep.* **12** 133
[59] Schichting H and Menzel D 1992 *Surf. Sci.* **272** 27
[60] Braun J, Fuhrmann D, Siber A, Gumhalter B and Wöll Ch 1998 *Phys. Rev. Lett.* **80** 125
[61] Unguris J, Bruch L W, Moog E R and Webb M B 1981 *Surf. Sci.* **109** 522
[62] Gibson K D and Sibener S J 1988 *J. Chem. Phys.* **88** 7893
[63] Bruch L W, Graham A P and Toennies J P 1998 *Mol. Phys.* **95** 579
[64] Caragiu M, Seyller T and Diehl R D 2003 *Surf. Sci.* **539** 165
[65] Ramseyer C, Pouthier V, Girardet C, Zeppenfeld P, Büchel M, Diercks V and Comsa G 1997 *Phys. Rev.* B **55** 13203
[66] Seyller T, Caragiu M and Diehl R D 2000 *Surf. Sci.* **454–456** 55
[67] Mason B F and Williams B R 1983 *Surf. Sci.* **130** 295
[68] Gibson K D and Sibener S J 1988 *J. Chem. Phys.* **88** 7862
[69] Toennies J P and Vollmer R 1989 *Phys. Rev.* B **40** 3495
[70] White J D, Lakin J V, Strauss M A and Diehl R D 1994 *J. Chem. Phys.* **101** 4445
[71] Pouthier V, Ramseyer C, Girardet C, Diercks V, Halmer R, David R and Zeppenfeld P 1998 *Phys. Rev.* B **57** 13149
[72] Suzanne J, Coulomb J P and Bienfait M 1975 *Surf. Sci.* **47** 204